



## LJMU Research Online

Hughes, ME, Pfeffer, JL, Martig, M, Reina-Campos, M, Bastian, N, Crain, RA and Kruijssen, JMD

The  $[\alpha/\text{Fe}]$ - $[\text{Fe}/\text{H}]$  relation in the E-MOSAICS simulations: its connection to the birth place of globular clusters and the fraction of globular cluster field stars in the bulge

<http://researchonline.ljmu.ac.uk/id/eprint/12007/>

### Article

**Citation** (please note it is advisable to refer to the publisher's version if you intend to cite from this work)

**Hughes, ME, Pfeffer, JL, Martig, M, Reina-Campos, M, Bastian, N, Crain, RA and Kruijssen, JMD (2019) The  $[\alpha/\text{Fe}]$ - $[\text{Fe}/\text{H}]$  relation in the E-MOSAICS simulations: its connection to the birth place of globular clusters and the fraction of globular cluster field stars in the bulge. Monthly Notices of the**

LJMU has developed **LJMU Research Online** for users to access the research output of the University more effectively. Copyright © and Moral Rights for the papers on this site are retained by the individual authors and/or other copyright owners. Users may download and/or print one copy of any article(s) in LJMU Research Online to facilitate their private study or for non-commercial research. You may not engage in further distribution of the material or use it for any profit-making activities or any commercial gain.

The version presented here may differ from the published version or from the version of the record. Please see the repository URL above for details on accessing the published version and note that access may require a subscription.

For more information please contact [researchonline@ljmu.ac.uk](mailto:researchonline@ljmu.ac.uk)

<http://researchonline.ljmu.ac.uk/>



# The $[\alpha/\text{Fe}]$ – $[\text{Fe}/\text{H}]$ relation in the E-MOSAICS simulations: its connection to the birth place of globular clusters and the fraction of globular cluster field stars in the bulge

Meghan E. Hughes<sup>1,2\*</sup>, Joel L. Pfeffer<sup>1</sup>, Marie Martig<sup>1</sup>, Marta Reina-Campos<sup>3</sup>,  
Nate Bastian<sup>1</sup>, Robert A. Crain<sup>1</sup> and J. M. Diederik Kruijssen<sup>3</sup>

<sup>1</sup>*Astrophysics Research Institute, Liverpool John Moores University, 146 Brownlow Hill, Liverpool L3 5RF, UK*

<sup>2</sup>*European Southern Observatory, Karl-Schwarzschild-Straße 2, D-85748 Garching, Germany*

<sup>3</sup>*Astronomisches Rechen-Institut, Zentrum für Astronomie der Universität Heidelberg, Mönchhofstraße 12-14, D-69120 Heidelberg, Germany*

Accepted 2019 November 26. Received 2019 November 4; in original form 2019 August 22

## ABSTRACT

The  $\alpha$ -element abundances of the globular cluster (GC) and field star populations of galaxies encode information about the formation of each of these components. We use the E-MOSAICS cosmological simulations of  $\sim L_*$  galaxies and their GCs to investigate the  $[\alpha/\text{Fe}]$ – $[\text{Fe}/\text{H}]$  distribution of field stars and GCs in 25 Milky Way–mass galaxies. The  $[\alpha/\text{Fe}]$ – $[\text{Fe}/\text{H}]$  distribution of GCs largely follows that of the field stars and can also therefore be used as tracers of the  $[\alpha/\text{Fe}]$ – $[\text{Fe}/\text{H}]$  evolution of the galaxy. Due to the difference in their star formation histories, GCs associated with stellar streams (i.e. which have recently been accreted) have systematically lower  $[\alpha/\text{Fe}]$  at fixed  $[\text{Fe}/\text{H}]$ . Therefore, if a GC is observed to have low  $[\alpha/\text{Fe}]$  for its  $[\text{Fe}/\text{H}]$  there is an increased possibility that this GC was accreted recently alongside a dwarf galaxy. There is a wide range of shapes for the field star  $[\alpha/\text{Fe}]$ – $[\text{Fe}/\text{H}]$  distribution, with a notable subset of galaxies exhibiting bimodal distributions, in which the high  $[\alpha/\text{Fe}]$  sequence is mostly comprised of stars in the bulge, a high fraction of which are from disrupted GCs. We calculate the contribution of disrupted GCs to the bulge component of the 25 simulated galaxies and find values between 0.3 and 14 per cent, where this fraction correlates with the galaxy’s formation time. The upper range of these fractions is compatible with observationally inferred measurements for the Milky Way, suggesting that in this respect the Milky Way is not typical of  $L_*$  galaxies, having experienced a phase of unusually rapid growth at early times.

**Key words:** methods: numerical – globular clusters: general – galaxies: evolution – galaxies: formation – galaxies: star clusters: general.

## 1 INTRODUCTION

The element abundances of stars and globular clusters (GCs) are powerful tools with which to extract information about the time and place of their formation, giving us an insight into how galaxies form and assemble. The element abundances of Milky Way (MW) GCs are often used to assess whether they formed in the MW or in a satellite galaxy that was later accreted. A powerful set of abundances are those of the  $\alpha$ -elements. The abundance ratio of  $\alpha$ -elements to iron,  $[\alpha/\text{Fe}]$ , is an important tracer of the relative contributions of Type-II/Ia supernovae (SNe), since only Type-II SN contribute to the production of  $\alpha$ -elements whereas both contribute to iron (Wheeler, Sneden & Truran 1989). This makes  $[\alpha/\text{Fe}]$ , together with  $[\text{Fe}/\text{H}]$ , a good tracer of the enrichment history

of a galaxy. For example, a star or GC with a high  $[\alpha/\text{Fe}]$  at fixed  $[\text{Fe}/\text{H}]$  indicates that its progenitor gas was enriched primarily with  $\alpha$ -elements synthesized and promptly released by Type-II SNe, whilst incorporating relatively little iron synthesized by Type-Ia SNe (Wheeler et al. 1989; McWilliam 1997). In many galaxies, low  $[\text{Fe}/\text{H}]$  stars that formed before Type-Ia SN enriched the interstellar medium (ISM) show a relatively constant  $[\alpha/\text{Fe}]$ . There is then a ‘knee’ in the  $[\alpha/\text{Fe}]$ – $[\text{Fe}/\text{H}]$  distribution, where stars begin to form from the Type-Ia SN-enriched material, followed by a downwards trend of decreasing  $[\alpha/\text{Fe}]$  as the ISM continues to be enriched by Type-Ia SN. Lower mass galaxies do not self-enrich as fast as higher mass galaxies and therefore the position of the ‘knee’ is shifted to lower  $[\text{Fe}/\text{H}]$  (e.g. Pritzl, Venn & Irwin 2005; Tolstoy, Hill & Tosi 2009).

The  $[\alpha/\text{Fe}]$ – $[\text{Fe}/\text{H}]$  distribution of field stars in cosmological simulations has been addressed in several recent studies. Mackereth et al. (2018) used the EAGLE simulations to investigate the

\* E-mail: M.Hughes1@2013.ljmu.ac.uk

$[\alpha/\text{Fe}]$ – $[\text{Fe}/\text{H}]$  distribution around the solar neighbourhood of 133 MW-like galaxies in terms of their stellar mass and kinematics. They found a diversity in the shape of the distributions, noting that only five per cent of them show a bimodal  $[\alpha/\text{Fe}]$  distribution, similar to that exhibited by the MW. The simulations indicate that this bimodality, in particular the appearance of a high- $\alpha$  sequence, occurs in galaxies that experience rapid growth at early epochs in response to a period of vigorous star formation triggered by the atypically early formation of their dark matter halo. The low- $\alpha$  sequence is then formed by a subsequent prolonged period of less intense star formation. The authors therefore concluded that the MW also underwent a rapid early growth, making it an atypical  $L^*$  galaxy. Grand et al. (2018) found  $[\alpha/\text{Fe}]$  bimodality in the disc populations of six MW-sized haloes in the Auriga simulations. Consistent with Mackereth et al. (2018), they attribute bimodality in the inner disc to a central starburst (caused by a gas rich merger), followed by less intense star formation. In the outer disc, they further attribute  $[\alpha/\text{Fe}]$  bimodality to early  $\alpha$ -rich star formation in a gas disc, followed by a shrinking of the disc that lowers the star formation rate. It is of particular interest that both studies attribute a high- $\alpha$  sequence to an early, rapid star formation episode (also see Kruijssen et al. 2019b).

In the MW GCs exhibit similar  $[\alpha/\text{Fe}]$  to field stars at fixed  $[\text{Fe}/\text{H}]$  (e.g. Pritzl et al. 2005). However, there are some Galactic GCs, such as Ruprecht 106 (Rup 106) and Palomar 12 (Pal 12) that have relatively low  $[\alpha/\text{Fe}]$  ratios for their  $[\text{Fe}/\text{H}]$  values with respect to both the MW field stars and other GCs. It has been hypothesized that these GCs have been captured from dwarf galaxies with a different chemical enrichment history to the MW (Lin & Richer 1992; Sneden 2004; Pritzl et al. 2005; Forbes & Bridges 2010). A similar offset is also seen when comparing stars in dwarf galaxies with the MW field stars (Pritzl et al. 2005; Tolstoy et al. 2009).

In the field stars, element abundances can be useful for finding groups of stars that were born in the same molecular cloud: this is called ‘chemical tagging’, a concept introduced by Freeman & Bland-Hawthorn (2002). Finding the stars that once belonged to bound clusters has become a major topic with the recent advances in Galactic surveys such as APOGEE (Majewski et al. 2017), Gaia-ESO (Gilmore et al. 2012), RAVE (Steinmetz et al. 2006; Zwitter et al. 2008; Siebert et al. 2011), and GALAH (De Silva et al. 2015; Buder et al. 2018). With these surveys it is possible to tag chemically hundreds of thousands of stars, making it possible to identify stars likely to have once been members of the same star cluster (e.g. Price-Jones & Bovy 2019). This same technique may be used to identify stars that once belonged to the same dwarf galaxy, providing an insight into the accretion history of the MW. On a larger scale, chemical tagging to find disrupted GCs and dwarf galaxies gives some clues about the early star formation process of the galaxy and its dynamical history (Ting, Conroy & Goodman 2015).

In addition to identifying stars that were born in the same molecular cloud, it is also interesting to consider more broadly the fraction of field stars that originated in GCs. If the fraction of stars formed in bound star clusters varies with the surface density of star formation (e.g. Kruijssen 2012), then the disrupted GC contribution to the thin disc, thick disc and bulge offers clues as to how each of these components formed. Stars that have formed within GCs can be identified by exploiting star-to-star abundance variations within GCs (e.g. Fernández-Trincado et al. 2019), known as multiple populations (e.g. Gratton, Sneden & Carretta 2004; Bastian & Lardo 2018). This has been carried out in the halo of the MW, where 2–3 per cent of halo stars were found to exhibit chemical signatures seen in GC stars (Martell et al. 2011; Carollo et al. 2013; Martell et al. 2016; Reina-Campos et al. 2019a). These studies

then attribute 4–17 per cent of halo stars as once being part of a GC, depending on the GC formation mechanism and the fraction of enriched stars initially within GCs. Schiavon et al. (2017) carried out a similar analysis in the MW bulge in a specific metallicity range of  $[\text{Fe}/\text{H}] < -1$  and, by finding nitrogen-enriched stars, concluded that 14 per cent of the stellar mass of the bulge came from disrupted GCs.

In a companion paper, we investigate the GC contribution to the halo of the 25 simulated MW–mass galaxies from the E-MOSAICS simulations. We find a median of 0.3 per cent of the mass in halo field stars formed in GCs, indicating that the disruption of GCs plays a sub-dominant roll in the build-up of galaxy stellar haloes (Reina-Campos et al. 2019a).

In this paper, we continue the study of  $\alpha$ -abundances in cosmological simulations using the 25 zoom-in E-MOSAICS simulations described by Pfeffer et al. (2018) and Kruijssen et al. (2019a) (for which the relevant details are discussed in Section 2), which enable us to follow the formation, evolution, and disruption of GCs alongside the evolution of their host galaxy. We discuss the differences and similarities between the field stars and GCs and the *in situ* and *ex situ* GCs in Section 3. In Section 4, we investigate the formation and disruption of GCs in the  $[\alpha/\text{Fe}]$ – $[\text{Fe}/\text{H}]$  plane. In Section 5, we present how the amount of GC disruption (particularly that in the bulge) can be related to the shape of the field star  $[\alpha/\text{Fe}]$ – $[\text{Fe}/\text{H}]$  distribution and subsequently the formation time of the galaxy. Finally, in Section 6 we present the conclusions of this work.

## 2 SIMULATIONS

For this work, we use the E-MOSAICS (MOdelling Star cluster population Assembly in Cosmological Simulations within EAGLE) suite of 25 zoom-in simulations of MW mass galaxies (Pfeffer et al. 2018; Kruijssen et al. 2019a). E-MOSAICS couples the MOSAICS subgrid model for star cluster formation and evolution (Kruijssen et al. 2011; Pfeffer et al. 2018) to the EAGLE (Evolution and Assembly of GaLaxies and their Environments) galaxy formation model (Crain et al. 2015; Schaye et al. 2015). These simulations follow the co-formation and evolution of galaxies and their star cluster populations in a cosmological context.

We focus here on the specific aspects of the simulations relevant to this work, namely the chemical abundances, the cluster formation efficiency (CFE), and cluster mass-loss. We refer the interested reader to Schaye et al. (2015), Pfeffer et al. (2018), and Kruijssen et al. (2019a) for full details of the EAGLE and MOSAICS models, respectively.

To follow the formation of a galaxy halo, the SUBFIND algorithm (Springel et al. 2001; Dolag et al. 2009) is used to identify subhaloes (galaxies) in the simulations, from which galaxy merger trees were constructed (see Pfeffer et al. 2018 for details). The merger trees enable us to assign a parent galaxy (we define ‘parent galaxy’ as the subhalo the particle was bound to prior to forming a star) to each GC and we can therefore label a GC’s formation as ‘*in situ*’ (its parent galaxy is the main progenitor) or ‘*ex situ*’ (its parent galaxy merged with the main progenitor).

EAGLE tracks the abundances of the 11 elements most important for radiative cooling. Following Segers et al. (2016) and Mackereth et al. (2018), we use  $[\text{O}/\text{Fe}]$  as a proxy for  $[\alpha/\text{Fe}]$ , since oxygen dominates the mass budget of  $\alpha$ -elements. Abundance ratios  $[a/b]$  are calculated as

$$[a/b] = \log_{10} \left( \frac{X^a}{X^b} \right) - \log_{10} \left( \frac{X_{\odot}^a}{X_{\odot}^b} \right). \quad (1)$$

We adopt solar fractions of  $X_{\odot}^{\text{O}}/X_{\odot}^{\text{Fe}} = 4.98$  and  $X_{\odot}^{\text{Fe}}/X_{\odot}^{\text{H}} = 0.0016$  from Wiersma, Schaye & Smith (2009), consistent with the cooling tables used in EAGLE.

MOSAICS adopts a star cluster formation model based on observations of young star clusters, under the assumption that young star clusters, open clusters and GCs share a common formation mechanism (see reviews by Longmore et al. 2014; Kruijssen 2014; Bastian 2016). When a star particle forms in the simulations, a fraction of its mass may form a star cluster population. Once this mass has been assigned to cluster formation, cluster masses are stochastically drawn from a Schechter (Schechter 1976) initial cluster mass function (ICMF) with an environmentally dependent truncation mass.<sup>1</sup>

Cluster populations for each star particle form with a local, environmentally varying CFE (i.e. the fraction of stars formed in bound clusters; Bastian 2008) and ICMF according to the models of Kruijssen (2012) and Reina-Campos & Kruijssen (2017), respectively. This cluster population inherits the age and chemical composition of its parent stellar particle.

The clusters lose mass due to stellar evolutionary mass-loss (in common with field stars) and dynamical processes. Mass-loss through stellar evolution is tracked for each stellar particle by the EAGLE model (Wiersma et al. 2009) and the lost mass is donated to neighbouring gas particles. For dynamical evolution, mass-loss from tidal shocks and two-body relaxation is included, as described in detail by Kruijssen et al. (2011), this redistributes the mass internally within the stellar particle from the bound to the field populations. Clusters are evolved down to  $100 M_{\odot}$ , after which they are assumed to be completely disrupted. Disruption of clusters by dynamical friction is applied to clusters at every snapshot in post-processing (since stellar particles may host clusters of different masses, see Pfeffer et al. 2018 for details). In this section and Section 3, we define a surviving GC as a star cluster in the simulations with a present-day mass greater than  $10^5 M_{\odot}$  and an age greater than 2 Gyr. In Section 4, our discussion is focused on the *initial* GC population that has now disrupted so we define a GC as a star cluster with an initial mass greater than  $10^5 M_{\odot}$  and an age greater than 2 Gyr. We use this age cut since we want to look for disrupted GCs in the field by utilizing multiple populations, a phenomenon which is known to exist in GCs older than 2 Gyr (Martocchia et al. 2018a).

The E-MOSAICS simulations reproduce many key observables of the MW and M31 GC populations, such as the specific frequency, the number of low-metallicity GCs ( $[\text{Fe}/\text{H}] < -1$ ), and the radial distribution of GCs. We direct the reader to Fig. 2 and the accompanying discussion of Kruijssen et al. (2019a) for an overview. In addition, the high-mass end of the simulated globular cluster mass function (GCMF) is in good agreement with that of the MW and M31. However, the simulations produce too many low-mass clusters (particularly at  $< 10^5 M_{\odot}$ ), most likely due to under disruption (Pfeffer et al. 2018). In this work, we account for this by limiting the GCs to  $> 10^5 M_{\odot}$  and providing extreme cases of complete disruption where necessary. Another observable reproduced by the E-MOSAICS simulations is the ‘blue tilt’, where more massive GCs are typically more metal rich. Using the E-MOSAICS simulations, Usher et al. (2018) reinterpreted the ‘blue tilt’ as an absence of

massive metal-poor GCs as a consequence of less-massive and therefore less-metal-rich galaxies not reaching sufficiently high interstellar gas surface densities to form massive GCs (see Kruijssen et al. 2019a for a similar but subtly different interpretation). The E-MOSAICS simulations also provide predictions for future observations, Reina-Campos et al. (2019b) find a median lookback time of GC formation to be 10.7 Gyr, approximately 2.5 Gyr earlier than that of the field stars. As a result, proto-GC formation is predicted to be the most prevalent between  $2 < z < 3$  (consistent with the peak of star formation history Madau & Dickinson 2014), a prediction that can be tested with *James Webb Space Telescope*.

### 3 THE $\alpha$ -ABUNDANCES OF GCS AND FIELD STARS

The  $\alpha$ -element abundances of GCs have been used to establish whether a GC is likely to have been formed *in situ* or *ex situ*, under the assumption that a GC with low  $[\alpha/\text{Fe}]$  at a fixed  $[\text{Fe}/\text{H}]$  (relative to the MW’s field stars) indicates an *ex situ* origin (e.g. Pritzl et al. 2005). The motivation for this follows from the assumption that GCs formed *ex situ* did so in a satellite galaxy with a longer gas consumption time-scale than the main progenitor. In particular, low-mass dwarf galaxies are expected to transition to low  $[\alpha/\text{Fe}]$  at lower  $[\text{Fe}/\text{H}]$  than more massive galaxies (Matteucci & Brocato 1990; Tolstoy et al. 2009). The underlying assumption to this classification is that the GC formation history is broadly representative of the field star formation history in all galaxies.

Pritzl et al. (2005) used a compilation of Galactic GCs with high-fidelity stellar abundance measurements and compared their  $[\alpha/\text{Fe}]$  abundances with those of the field stars. They find that GCs follow the abundances of field stars reasonably well, with a few exceptions. In particular, they suggest that Ter 7, Pal 12, and Rup 106 have an extra-galactic origin based on their lower  $[\alpha/\text{Fe}]$  abundances. This is also suggested in other studies where Ter 7 (Da Costa & Armandroff 1995) and Pal 12 (Dinescu et al. 2000) are inferred to be associated with the tidally disrupting Sagittarius dwarf galaxy. It has been suggested that Rup 106 is of extragalactic origin, although its parent galaxy is still debated (Bellazzini, Ferraro & Ibata 2003; Law & Majewski 2010; Forbes & Bridges 2010; Massari, Koppelman & Helmi 2019). Other MW GCs with low  $[\alpha/\text{Fe}]$  suggesting extragalactic origin include NGC 5694 (Lee, López-Morales & Carney 2006; Mucciarelli et al. 2013) and Pal 1 (Monaco et al. 2011; Sakari et al. 2011). There is also evidence that the GCs in the Fornax dwarf galaxy have lower  $[\alpha/\text{Fe}]$  when compared to the MW GCs (Larsen, Brodie & Strader 2012). Also, Cohen (2004) and Tautvaišienė et al. (2004) concluded that the known Sagittarius GCs follow the  $[\alpha/\text{Fe}]$  trend of the known Sagittarius field stars.

We present in Fig. 1 a subset of the E-MOSAICS galaxies with a range of shapes in  $[\alpha/\text{Fe}]$ – $[\text{Fe}/\text{H}]$  to highlight key points in the differences and similarities between galaxies. These are MW06, MW12, MW13, MW18, and MW23 in table 1 of Kruijssen et al. (2019a). The contours represent the field stars and the GCs are overplotted as red or blue points depending if they formed *in situ* or *ex situ*, respectively. Unless otherwise stated, when we refer to ‘field stars’ in this work we are referring to all stellar particles that are bound to the main subhalo. When calculating the mass of the field stars, the mass of the GC population associated with the stellar particle is omitted. In all the galaxies, both the field stars and the GCs show a decline of  $[\alpha/\text{Fe}]$  with increasing  $[\text{Fe}/\text{H}]$ . From left to right, the panels show field star distributions ranging from a smooth decline to being clearly bimodal at fixed metallicity

<sup>1</sup>So as to not impose an upper limit on the cluster mass, the cluster masses are allowed to exceed the mass of the particle. This is justified because occasionally, the truncation mass of the ICMF exceeds the mass of a stellar particle in these high-resolution simulations.

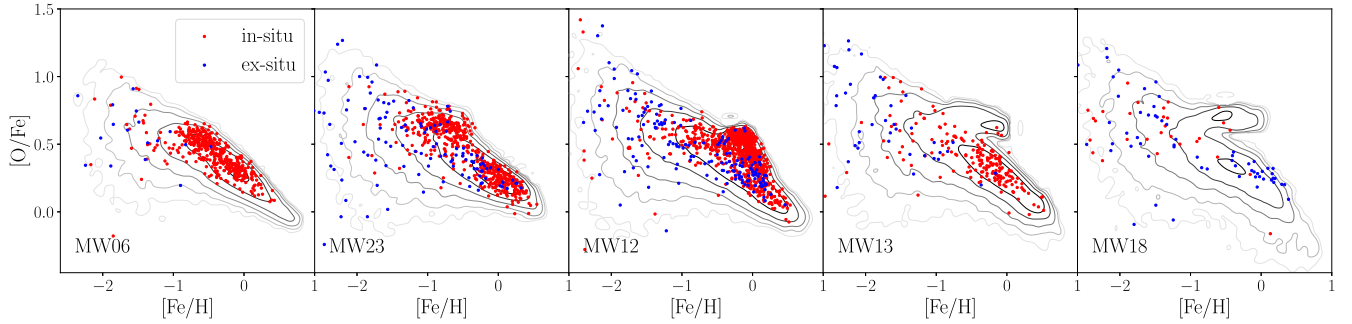


**Figure 1.** Five of the E-MOSAICS galaxies in  $[\alpha/\text{Fe}]$ – $[\text{Fe}/\text{H}]$  space, chosen to illustrate the diversity of the  $z = 0$   $[\alpha/\text{Fe}]$ – $[\text{Fe}/\text{H}]$  distributions. The contours represent the field stars and the points represent the *in situ* (red) and *ex situ* (blue) GCs.

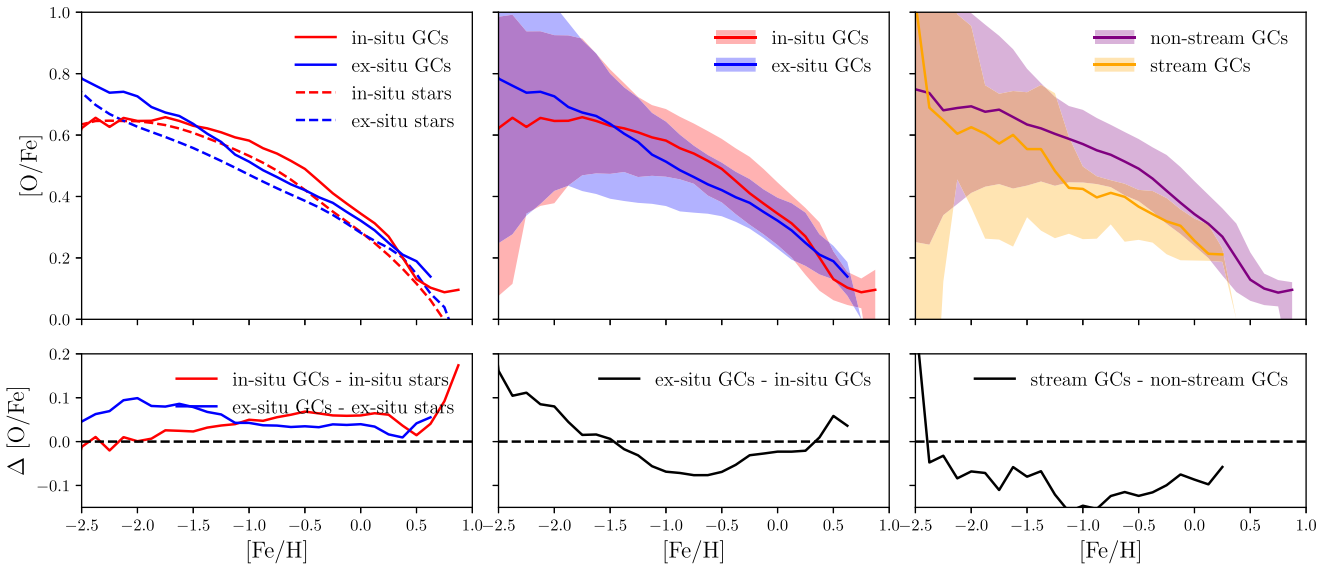


**Figure 2.** Top left: The median  $[\text{O}/\text{Fe}]$  as a function of metallicity of the *in situ* and *ex situ* field stars and GCs in all 25 galaxies. Top middle: The median  $[\text{O}/\text{Fe}]$  as a function of metallicity of the *in situ* and *ex situ* GCs in all 25 galaxies. Top right: The median  $[\text{O}/\text{Fe}]$  as a function of metallicity of the GCs on streams and not on streams in the 15 MW-like galaxies identified in Hughes et al. (2019). The shaded regions show the 16th and 84th percentiles and the lines are a running median of  $[\text{O}/\text{Fe}]$  in  $[\text{Fe}/\text{H}]$  bins of 0.5 dex with a difference of 0.125 dex between each bin. The bottom panels show the differences in  $[\text{O}/\text{Fe}]$  between the subsets of stars or GCs for each  $[\text{Fe}/\text{H}]$  bin. All panels only include bins with more than 5 GCs to avoid poor sampling issues.

(in the range  $-1 < [\text{Fe}/\text{H}] < 0$ ). Mackereth et al. (2018) used the EAGLE simulations to investigate the  $[\alpha/\text{Fe}]$  abundances of the field stars around the solar radius (thus excluding stars in the bulge) in a sample of MW-like galaxies. They also found bimodality in 5 per cent of their galaxies and attribute the appearance of bimodality to a phase of rapid growth early in the galaxy’s formation history – we investigate this explanation and its relation to GCs in Section 5.

The first thing we note is that the abundances of the GCs closely trace the abundances of the field star population; however, similarly to the MW there are some clear exceptions. All of the galaxies shown in Fig. 1 host a small population of GCs that have low  $[\alpha/\text{Fe}]$  for a given  $[\text{Fe}/\text{H}]$ . However, contrary to what is assumed for the MW, this population of GCs is not universally *ex situ*. In E-MOSAICS GCs, follow the abundance trends of the field stars by construction (there cannot be a GC without a star particle), but where the GCs form and how they evolve in the simulation may impart biases on the properties of the star particles that still hold a GC at  $z = 0$ . We investigate these points further by stacking all 25 MW-like galaxies and looking for systematic trends in Fig. 2.

To test whether GCs follow the abundance trends of the field stars in our simulations, we show the median  $[\text{O}/\text{Fe}]$  for fixed bins of  $[\text{Fe}/\text{H}]$  of the *in situ* (red) and *ex situ* (blue) GCs and field stars of the 25 galaxies (the top left-hand panel of Fig. 2). Both field stars (dashed lines) and GCs (solid lines) show a decrease in the median  $[\text{O}/\text{Fe}]$  with increasing  $[\text{Fe}/\text{H}]$ , a similar trend to that seen in the MW field stars and GCs (e.g. Hayden et al. 2015). We also find that the GCs follow the general trend of the field stars, but they are offset to higher  $[\text{O}/\text{Fe}]$ . We quantify this difference in the bottom left-hand panel, where we show the difference in median  $[\text{O}/\text{Fe}]$  between stars and GCs for both the *in situ* and *ex situ* populations. This panel shows that the GC  $[\text{O}/\text{Fe}]$  is always greater than that of the field stars by  $\sim 0.05$  dex. We expect GCs to show higher  $[\text{O}/\text{Fe}]$  because, in the MOSAICS model, GCs are formed in high-density environments and high-density environments induce shorter gas consumption times (the Appendix; Mackereth et al. 2018, fig. 4; Tacconi et al. 2018), which in turn leads to higher  $[\text{O}/\text{Fe}]$ . The gas consumption time is an estimate of the time a star-forming gas particle resides in the ISM before becoming a star particle. It can vary significantly across a single galaxy due to variations in

pressure. A correlation between gas consumption time and  $[\alpha/\text{Fe}]$  is not necessary, because such correlation only arises if a parcel of gas is self-enriched (i.e. there is no dilution from gas infall, the Fe and  $\alpha$ -elements produced by stellar evolution are not ejected to large distances, and there is no large-scale radial mixing of gas within the galaxy). In the EAGLE simulation, a correlation between gas consumption time and  $[\alpha/\text{Fe}]$  has been demonstrated by Mackereth et al. (2018, their fig. 4). This arises because metals produced by stellar evolution are returned locally (using the SPH kernel), and because gas consumption time-scales are similar to the time-scales of the Type-IaSNe delay time distribution.

To further study the difference in the  $\alpha$ -abundances of the *in situ* and *ex situ* GCs, we show their median  $[\text{O}/\text{Fe}]$  values as a function of  $[\text{Fe}/\text{H}]$  in the middle panel of Fig. 2, where the shaded region shows the 16th and 84th percentile range. Although the *ex situ* GCs show, on average, systematically lower  $[\text{O}/\text{Fe}]$ , the distributions heavily overlap and the difference between the medians is smaller than the  $1\sigma$  ranges. The middle bottom panel of Fig. 2 shows the difference between the *in situ* and *ex situ* GC median  $[\text{O}/\text{Fe}]$ . There is a range of  $[\text{Fe}/\text{H}]$  ( $-1.2 < [\text{Fe}/\text{H}] < -0.25$ ) in which *ex situ* GCs have a lower median  $[\text{O}/\text{Fe}]$  than *in situ* GCs, but outside of this range  $[\text{O}/\text{Fe}]$  is similar or *ex situ* GCs have higher  $\alpha$ -enhancement (particularly for  $[\text{Fe}/\text{H}] < -1.8$ ). Therefore, we cannot say definitively that *ex situ* GCs show lower  $\alpha$ -abundances at all  $[\text{Fe}/\text{H}]$ . However, the *ex situ* GCs in these simulations are identified as any GC that has been accreted on to a central galaxy over its full formation history. This means that some of the *ex situ* GCs were formed in progenitors that were accreted very early on in the galaxy's formation history, and consequently they would most likely be identified as *in situ* GCs in chemical and kinematic studies. Dwarf galaxies accreted early tend to have more rapid formation histories (in terms of the time it takes them to reach a maximum mass) than those accreted late (Mistani et al. 2016); therefore, we would expect them to have higher  $[\alpha/\text{Fe}]$  abundances. Therefore, it would be prudent for us to examine an alternative definition of an *ex situ* GC to facilitate a more direct comparison with observations of GCs in the MW.

The most direct evidence for accretion in the MW comes in the form of stellar streams, therefore we complement the *in situ/ex situ* comparison with a stream/non-stream comparison. For that, we use the sample of stellar streams in 15 of the E-MOSAICS MW-mass galaxies from Hughes et al. (2019), which were visually identified in 2D projections of the stellar particles of accreted galaxies. We show their  $[\text{O}/\text{Fe}]$  abundances in the right-hand panel of Fig. 2 and quantify the differences in the bottom right-hand panel. This panel shows that the stream GCs have consistently lower  $[\text{O}/\text{Fe}]$  abundances than the non-stream GCs. At  $[\text{Fe}/\text{H}] = -1$ , the difference between the stream and the non-stream GCs is double that of the difference between the *ex situ* and *in situ* GCs. Therefore, we can conclude that if we observe a GC in the halo of a galaxy that belongs to a stream, there is a high probability that it will be  $\alpha$ -poor relative to the main GC population. This supports the conclusion of works that state that *ex situ* GCs should exhibit lower  $[\alpha/\text{Fe}]$  at fixed  $[\text{Fe}/\text{H}]$  than *in situ* GCs (e.g. Pritzl et al. 2005); however, we would revise this conclusion to state that we can distinguish recently accreted GCs this way, i.e. that high  $[\alpha/\text{Fe}]$  does not necessarily imply that a GC formed *in situ*, as at low metallicity most GCs form with high  $[\alpha/\text{Fe}]$ . We can also conclude that if we were to find a low  $[\alpha/\text{Fe}]$  GC in the halo of a galaxy it is likely to have been accreted relatively recently and could be a signpost for the presence of an associated disrupting dwarf galaxy. The lower  $\alpha$ -abundance of these accreted stars and GCs is not driven by their *ex situ* origin in itself, but by the fact that they formed and accreted recently.

## 4 THE $[\alpha/\text{Fe}]$ – $[\text{Fe}/\text{H}]$ DISTRIBUTION OF FIELD STARS AND ITS CONNECTION TO THE FORMATION AND DISRUPTION OF GCs

### 4.1 Cluster formation and disruption across the $[\alpha/\text{Fe}]$ – $[\text{Fe}/\text{H}]$ plane

Section 3 shows us that the  $\alpha$ -abundances of a galaxy's GCs encode information about the formation and assembly of the galaxy's GC population. We now focus on what we may learn about the contribution of disrupted GCs to the galaxy's field star population from their  $\alpha$ -abundances. In Fig. 1, MW13 and MW18 show a bimodal  $[\text{O}/\text{Fe}]$  distribution in their field stars at  $[\text{Fe}/\text{H}] \approx -0.25$ ; however, there are relatively few GCs in the high  $[\alpha/\text{Fe}]$  sequence compared to the low  $[\alpha/\text{Fe}]$  sequence. This motivates investigation of the  $[\alpha/\text{Fe}]$ – $[\text{Fe}/\text{H}]$  plane in terms of GC formation and disruption.

#### 4.1.1 GC formation

We first focus on the formation of GCs through the CFE. The CFE governs the fraction of star formation that yields bound clusters (see Adamo & Bastian 2018 for a recent review). The CFE increases with star formation rate surface density (Adamo et al. 2015) and in the E-MOSAICS simulations it scales with the natal gas pressure. E-MOSAICS uses the environmentally dependent description of the CFE from the Kruijssen (2012) model, which relates the fraction of star formation into bound stellar clusters to the properties of the ISM – bound clusters form most efficiently at the high-density end of the hierarchically structured ISM.

The first row of Fig. 3 shows a 2D histogram of the stellar particles in the  $[\text{O}/\text{Fe}]$ – $[\text{Fe}/\text{H}]$  space coloured by the CFE associated with their birth cloud (or 'natal gas'). The CFE ranges from a few per cent to 80 per cent, depending on the location in  $[\alpha/\text{Fe}]$ – $[\text{Fe}/\text{H}]$  space. As the stellar  $[\alpha/\text{Fe}]$ – $[\text{Fe}/\text{H}]$  distribution becomes more bimodal (Fig. 1, from left to right), the high CFE feature in the galaxy (Fig. 3, second row) becomes more pronounced in the high- $\alpha$  sequence. The CFE is dependent on the density of the natal gas of the stellar particle (through the natal pressure, due to the equation of state imposed on dense, star-forming gas), with higher densities leading to a higher CFE. Therefore, the high- $\alpha$  sequence must form from material with increased natal gas pressure, meaning that the stars form from gas with short gas consumption times (see the Appendix and Mackereth et al. 2018 for details).

However, as discussed earlier, the bimodal galaxies MW13 and MW18 have a lack of GCs in their high  $[\alpha/\text{Fe}]$  sequence, even though this is the same area of  $[\alpha/\text{Fe}]$ – $[\text{Fe}/\text{H}]$  space where the CFE is the highest. This means that although there is a clearly defined area in this plane where the galaxy is forming a large number of GCs, these GCs do not survive to  $z = 0$ . Therefore, we now investigate GC disruption across the  $[\alpha/\text{Fe}]$ – $[\text{Fe}/\text{H}]$  plane.

#### 4.1.2 GC disruption

The region of high CFE in the  $[\alpha/\text{Fe}]$ – $[\text{Fe}/\text{H}]$  plane tells us that the stars and GCs that form in this region do so in a high-density environment. However, tidal shocks are also more prevalent in high-density environments and can efficiently disrupt the nascent cluster. This is the 'cruel cradle effect' described by Kruijssen et al. (2012) and means that where a galaxy is likely to form many clusters, it is also likely to disrupt them. Dynamical friction also removes many of the most massive clusters that are not disrupted by tidal shocks, particularly in the centres of galaxies.

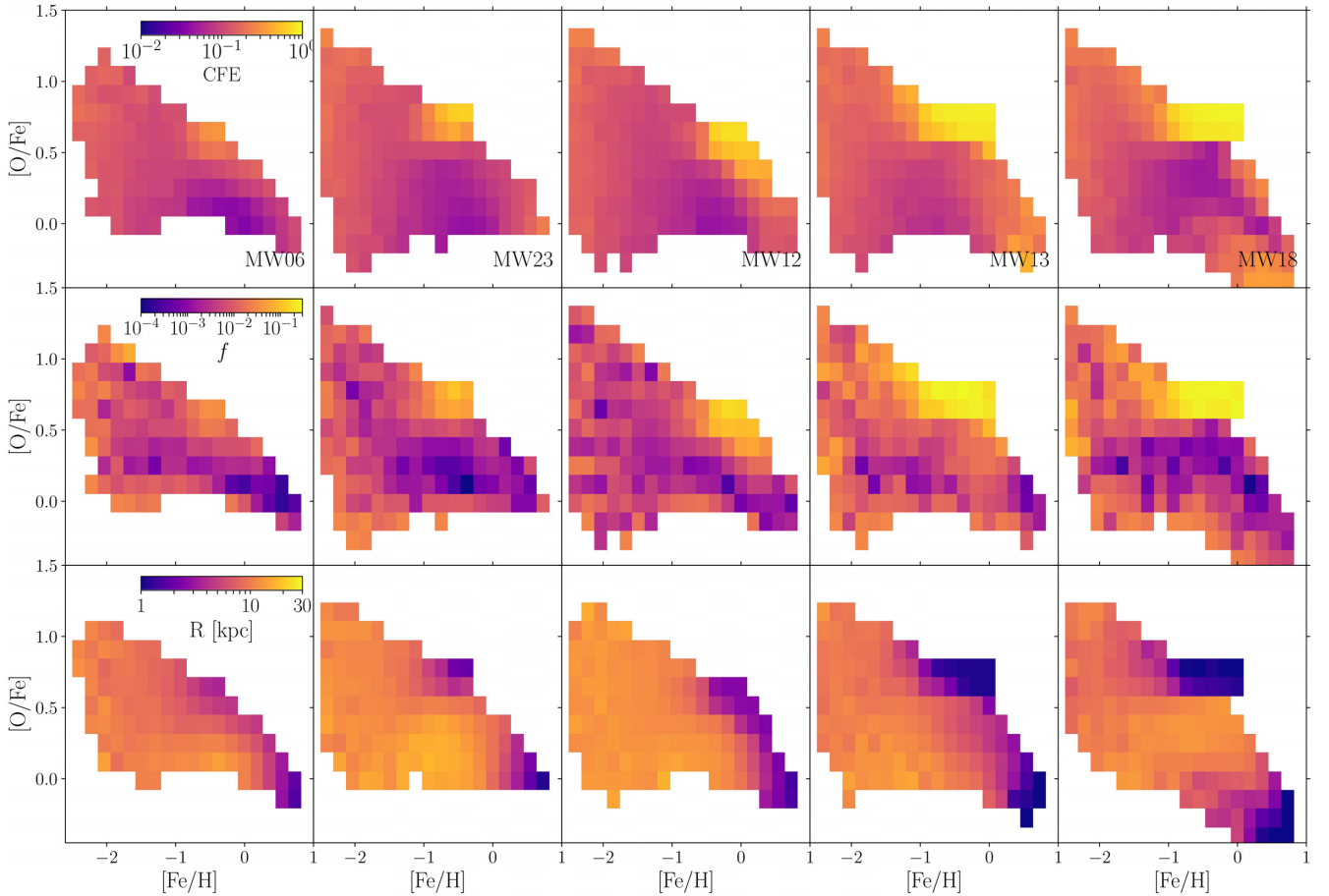


**Figure 3.** The [O/Fe]–[Fe/H] relation for five of the simulated galaxies. Each panel shows a 2D histogram of the stars in the galaxy coloured by, the CFE, the fraction of stars that were born in GCs but now reside in the field ( $f$ ) and the galactocentric radius of the stars at  $z = 0$  ( $R$ ). In the last row, only the stars from the inner 30 kpc are shown.

The combination of the cruel cradle effect and dynamical friction explains the absence of GCs in the same location in  $[\alpha/\text{Fe}]$ –[Fe/H] space, where the CFE is high in Fig. 3.

We can make a measurement of the fraction of the stars that formed in bound massive clusters similar to present-day GCs but now reside in the field. For this purpose, we revise slightly our definition of a GC to that of a star cluster with an *initial mass* greater than  $10^5 M_\odot$  and an age greater than 2 Gyr. The second row of Fig. 3 shows a 2D histogram of all the stellar particles in the galaxy weighted by the fraction of their mass that once belonged to a GC that has since dissolved into the field star population,

$$f = \frac{\sum_i^{N_*} (M_{\text{GC},\text{init}} \times \text{SML} - M_{\text{GC},\text{final}})}{\sum_i^{N_*} M_{*,\text{field}}}, \quad (2)$$

where  $M_{\text{GC},\text{init}}$  is the initial total mass in GCs,  $M_{\text{GC},\text{final}}$  is the final total mass in GCs,  $M_{*,\text{field}}$  is the final total mass field star population in the stellar particles and the factor  $\text{SML} = M_{*,\text{final}}/M_{*,\text{init}}$  corrects the initial total mass in GCs for stellar evolutionary mass-loss (such that we are only considering dynamical mass-loss). We include mass-loss from tidal shocks and two-body relaxation but not the complete removal of clusters by dynamical friction. Dynamical friction is omitted, since we assume that this mass will quickly sink to the centre of the galaxy potentially contributing to the nuclear

star cluster<sup>2</sup> (e.g. Antonini 2013). Therefore, these stars would not be easily identifiable through chemical tagging studies of the field star population of the Galaxy.

Some of the galaxies show a clearly defined region of [O/Fe]–[Fe/H] space where up to 30 per cent of the field stars were born in GCs. This region of high  $f$  is the same as the region of high CFE and overlaps with the high [O/Fe] sequence in the galaxies that show bimodality in the top row. Therefore, we show that in some galaxies, some stars are born in high-density regions of star-forming gas, which means that for a given [Fe/H] their [O/Fe] will be high. Due to the high densities, it is likely that these stars will form in bound clusters, but because of the ‘cruel cradle effect’ a high fraction of these clusters will also be fully or partially disrupted. Hence, in some galaxies, there is expected to be a region in  $[\alpha/\text{Fe}]$ –[Fe/H] space where a high fraction of field stars were originally born in GC-like clusters. This has implications for chemical tagging studies and will be discussed in detail in Section 5.

#### 4.2 Galactocentric position in the $[\alpha/\text{Fe}]$ –[Fe/H] plane

We investigate whether there is a radial dependence on where stellar particles will be distributed in  $[\alpha/\text{Fe}]$ –[Fe/H] space. In the bottom

<sup>2</sup>Any potential increase in tidal disruption due to a shrinking orbit cannot be captured in the present model.

row of Fig. 3, we show a 2D histogram of the stellar particles within 30 kpc of the centre of the galaxy, coloured by their galactocentric (spherical) radius. The region of  $[O/Fe]$ – $[Fe/H]$  space that shows the highest fraction of disrupted GC stars ( $f$ ) resides at the centre, or bulge, of the galaxy. This is expected, since the centres of galaxies usually show the highest pressures due to the radial pressure gradient of the gas (see e.g. fig. 8 of Crain et al. 2015). Due to the high  $[\alpha/Fe]$  sequence of interest being concentrated towards the centre of these galaxies, we consider just the bulge of the galaxy in Section 5.

## 5 THE FRACTION OF FIELD STARS IN THE BULGE ORIGINATING IN GCS

### 5.1 Bulge stars from disrupted GCs in E-MOSAICS

We found in Section 4 that the high  $[\alpha/Fe]$  sequence of stellar particles shown in Fig. 3 mostly reside close the centre of the galaxies. We therefore target the bulges of the 25 E-MOSAICS galaxies in the rest of this analysis, with a focus on the contribution of disrupted GCs to the formation of the bulge. Since the size of the bulge varies for each galaxy we make a radius and orbital circularity cut. We define the orbital circularity as in Abadi et al. (2003),  $\epsilon_J = J_z/J_c(E)$  (i.e. the angular momentum relative to the angular momentum of a circular orbit), where  $\epsilon = 1$  describes a perfectly circular orbit. The field stars in the bulge are therefore defined as the stellar particles within the stellar half mass radius with  $\epsilon_J < 0.5$  (Sales et al. 2015).

We can now determine the contribution of disrupted GCs to the stellar population of the bulge, in the form of the fraction of field stars in the bulge that were born in a GC ( $f_{\text{bulge}}$ ). The E-MOSAICS galaxies host too many GCs at  $z = 0$  due to under disruption (Pfeffer et al. 2018; Kruijssen et al. 2019a). For this reason, our fractions should be considered as lower limits. Therefore, we also show the extreme upper limits on  $f_{\text{bulge}}$ , where we assume that every GC formed in the bulge of the galaxy becomes disrupted i.e. no GC survives to the present day in the bulge. Such an extreme assumption does not affect the general trend of the simulations.

We show  $f_{\text{bulge}}$  for all 25 galaxies in the top panel of Fig. 4 and see that there is a large range in the value of  $f_{\text{bulge}}$ , from 0.3 to 14 per cent. This fraction is dependent on the time at which the total stellar mass of all progenitors of that galaxy reaches half of the  $z = 0$  mass ( $z_{\text{formation}}$ , De Lucia et al. 2006; Qu et al. 2017), such that galaxies that formed faster have higher  $f_{\text{bulge}}$ .

We also group the galaxies by the shape of their stellar contours in  $[\alpha/Fe]$ – $[Fe/H]$  space (like those shown in Fig. 1). We place each galaxy into one of three categories:

- (i) No bimodality, where there is a smooth decline in  $[O/Fe]$  for increasing  $[Fe/H]$  (e.g. MW06).
- (ii) Intermediate bimodality, where there is a small bump or a slight increase in  $[O/Fe]$  for a given metallicity (e.g. MW23 and MW12).
- (iii) Clear bimodality, where there are two distinct  $[O/Fe]$  sequences at a given metallicity (e.g. MW13 and MW18).

We conclude that the most bimodal galaxies are those that have faster formation times and higher  $f_{\text{bulge}}$ . This is to be expected since, from Section 4, the high  $[\alpha/Fe]$  sequence in the bimodal galaxies is formed from a high pressure environment close to the centre of the galaxy, where GCs are efficiently formed and subsequently disrupted.

We also present the metallicity dependent  $f_{\text{bulge}}$  in Fig. 5. Here,  $f_{\text{bulge}}$  is calculated in  $[Fe/H]$  bins of 0.5 dex and the median and the

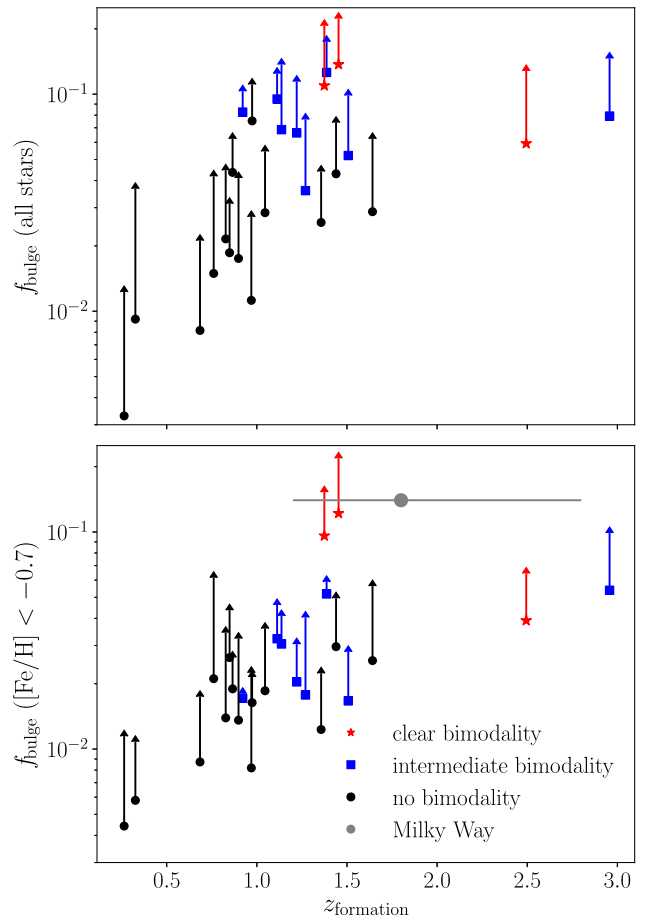


**Figure 4.** The fraction of field stars in the bulge which were born in GCs ( $f_{\text{bulge}}$ ) as a function of the redshift ( $z_{\text{formation}}$ ) at which all progenitors together have attained half of the  $z = 0$  stellar mass (this is effectively the median age or median formation redshift of all stars in the galaxy at  $z = 0$ ). The different symbols represent the degree of bimodality the field stars show in the  $[O/Fe]$ – $[Fe/H]$  plane, from definite bimodality (stars), to intermediate bimodality (squares) to no bimodality at all (circles). The data are shown as lower limits due to the under disruption of GCs in E-MOSAICS. The upper limits (at the tips of the arrows) show the extreme assumption that no GC survives in the bulge. Top panel:  $f_{\text{bulge}}$  across all field stars in the bulge. Bottom panel:  $f_{\text{bulge}}$  for field stars below  $[Fe/H] < -0.7$  to match the selection when deriving  $f_{\text{bulge}}$  for the MW. The grey data point indicates the bulge mass fraction from GCs derived by Schiavon et al. (2017) for the formation redshift of the MW inferred from the age–metallicity distribution of its GC population by Kruijssen et al. (2019b).

16th–84th percentile range of the galaxies grouped by their level of bimodality is shown. For all galaxies, GC disruption and the contribution of GCs to the field star population increases towards higher metallicities for  $[Fe/H] < -0.5$ . The clearly bimodal galaxies show the highest and most metal-poor peak. The intermediate bimodal galaxies show a smaller and slightly more metal-rich peak and the galaxies with no bimodality show a relatively flat  $f_{\text{bulge}}$  with increasing  $[Fe/H]$ . Fig. 4 allows us to conclude that the MW has a high fraction of disrupted GCs in its bulge, consistent with the most bimodal simulated galaxies. We therefore use the most bimodal galaxies in Fig. 5 to predict that the stars from disrupted GCs in the bulge of the MW will show the highest fraction around  $[Fe/H] \approx -1$ .

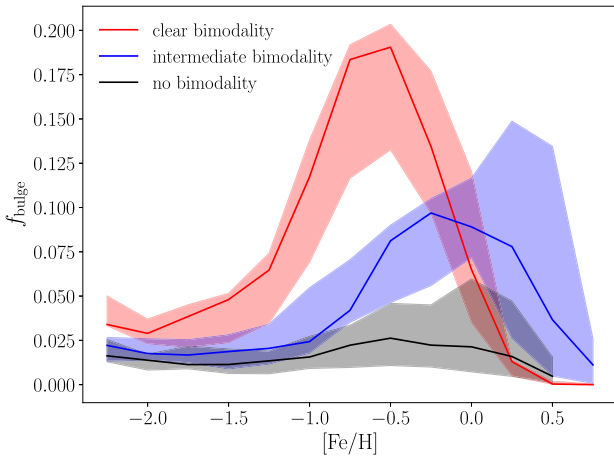


**Figure 5.** The fraction of field stars in the bulge that were contributed by GCs ( $f_{\text{bulge}}$ ) in 0.5 dex  $[\text{Fe}/\text{H}]$  bins. The solid lines show the running median and the shaded regions represent the 16–84th percentile range. The galaxies are stacked by the level of bimodality their stars show in the  $[\alpha/\text{Fe}]$ – $[\text{Fe}/\text{H}]$  plane, coloured as in Fig. 4.  $f_{\text{bulge}}$  peaks higher and at lower metallicities in galaxies with clear  $[\alpha/\text{Fe}]$  bimodality.

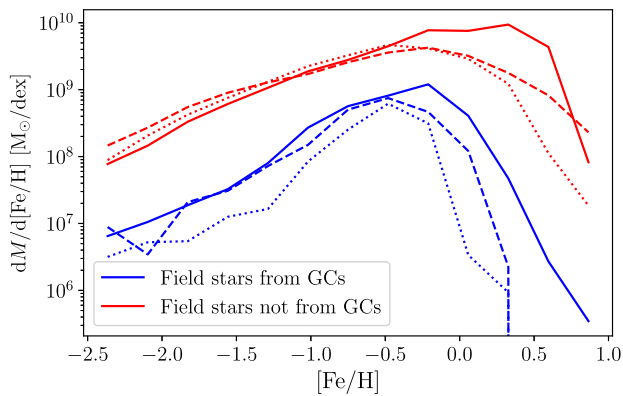


**Figure 6.** The MDF of field stars in the bulges of the three E-MOSAICS galaxies that show bimodal  $[\alpha/\text{Fe}]$  at a given  $[\text{Fe}/\text{H}]$ , these are MW13 (solid line), MW18 (dashed line), and MW21 (dotted line). The stars are split by whether they were born in a GC (blue lines) or not (red lines).

## 5.2 Comparison with the MW

Searching for stars from disrupted GCs in the bulge of the MW is something that has been done with large-scale surveys of galactic stars. These searches mainly focus on finding populations of nitrogen-rich stars (Schiavon et al. 2017).

Whilst some stars in GCs show the same chemical abundances as those found in the field (first population, FP), others show enhancements or depletions in some elements, such as a nitrogen enhancement (second population, SP, e.g. Carretta et al. 2009; for a recent review, see Bastian & Lardo 2018).

It is interesting here to address the effect the formation time-scales of multiple populations may have on our comparison with the MW bulge. The main theories for the origin of multiple populations in GCs suggest that the formation of SP stars happens on time-scales  $< 300$  Myr. For scenarios invoking enrichment by massive stars, the time-scales for SP star formation are  $< 5$ – $10$  Myr (e.g. Gieles et al. 2018). For the asymptotic giant branch (AGB) scenario, the time-scale to form SP stars is  $< 100$  Myr, as this is the time-scale for the

first Type-Ia SNe to stop further generations of stars forming within the cluster (D’Ercole et al. 2008). Furthermore, observations also give us some constraint on the relative formation times of FP and SP stars. Ancient GCs show that the age difference between the two populations is  $< 200$  Myr and consistent with 0 Myr (Marino et al. 2012). Younger GCs also show a similar difference with an age difference calculated for NGC 1978 of  $1 \pm 20$  Myr (Martocchia et al. 2018b). Therefore, both theoretical and observational evidence suggest that GC disruption happens after multiple populations form and we can therefore directly compare the nitrogen-rich stars in the MW with disrupted GCs in the simulations without adding any extra calculations for the formation times of the nitrogen-rich stars.

Schiavon et al. (2017) used APOGEE to find a population of nitrogen-rich stars in the bulge of the MW. Restricting their selection to stars below  $[\text{Fe}/\text{H}] = -1$ , they found that 7 per cent of the field stars in the bulge are nitrogen enhanced. Although they advance multiple explanations for the origin of these stars, their preferred explanation is that they are remnants of disrupted GCs. Schiavon et al. (2017) then assume equal numbers of first and second population stars are lost from GCs and calculate that 14 per cent of field stars in the bulge (within this metallicity selection) formed in a GC.

In order to fairly compare the results from the E-MOSAICS simulation to that of the MW, we also make a metallicity selection for the stars in the bulges of the simulations. Due to the metallicities in the EAGLE simulations being overestimated (Schaye et al. 2015), we make a metallicity cut-off  $[\text{Fe}/\text{H}] < -0.7$  to compare with the metallicity cut-off  $[\text{Fe}/\text{H}] < -1$  in Schiavon et al. (2017). We show this in the bottom panel of Fig. 4, using for the MW,  $z_{\text{formation}} = 1.8^{+1.0}_{-0.6}$  (Kruijssen et al. 2019b). Although the metallicity cut reduces the  $f_{\text{bulge}}$  calculation for most galaxies, the MW is consistent with the subset of E-MOSAICS galaxies with a bimodal  $[\alpha/\text{Fe}]$  distribution, fitting with the observation that the MW also exhibits an  $[\alpha/\text{Fe}]$  bimodality (Fuhrmann 1998; Adibekyan et al. 2012; Hayden et al. 2015). We note here that Schiavon et al. (2017) did not make any orbital cuts in their selection; however, when we do not include the circularity cut, there is no significant change in Fig. 4 and therefore we keep this in our analysis for consistency.

Schiavon et al. (2017) also present the metallicity distribution of their sample of nitrogen-enriched stars. The metallicity distribution function (MDF) peaks at  $[\text{Fe}/\text{H}] \sim -1$ , whereas the MDF of the bulge field stars begins to decline at this metallicity (Schiavon et al. 2017, fig. 9). Therefore, we conclude that for the MW  $f_{\text{bulge}}$  will indeed peak at  $[\text{Fe}/\text{H}] \sim -1$  as predicted from the simulations in the previous section. In Fig. 6, we present the MDF of field stars in the bulge of the three galaxies in our sample that are classified as bimodal in their  $[\alpha/\text{Fe}]$  distributions (MW13, MW18, and MW21). The field stars are coloured by whether they were once bound to GC (blue lines) or not (red lines). Schiavon et al. (2017) present a similar figure in which they show the metallicity distributions of nitrogen-rich and nitrogen-normal stars. Similar to the distribution shown in Schiavon et al. (2017), the ex-GC stars in the E-MOSAICS simulations show a more peaked distribution than that of the field stars not from GCs. Also similar to Schiavon et al. (2017) the ex-GC stars peak at a lower metallicity than the stars not born in GCs (albeit at a higher metallicity than the MW).

Our findings therefore corroborate the conclusion of Schiavon et al. (2017) that the population of nitrogen-enriched stars found in the bulge of the MW are likely to be from disrupted clusters. However, such a large fraction (14 per cent) of stars in the bulge originating in clusters is rare in the E-MOSAICS simulations, with only two of the galaxies showing fractions greater than 10 per cent. In the context of our findings, such a high nitrogen-enhanced

fraction of bulge stars constitutes further evidence that the MW formed unusually early in cosmic history, given its halo mass (also see Mackereth et al. 2018 and Kruijssen et al. 2019b).

## 6 CONCLUSIONS

This work uses the E-MOSAICS simulations to investigate the  $[\alpha/\text{Fe}]$ – $[\text{Fe}/\text{H}]$  distribution of a galaxy’s field stars and GCs. Fig. 1 reveals many interesting features in the  $[\alpha/\text{Fe}]$ – $[\text{Fe}/\text{H}]$  space of the E-MOSAICS galaxies, namely, bimodal distributions and a lack of GCs in the high  $\alpha$ -sequence. Therefore, we use 25 MW-like galaxies and their GC populations to understand what their  $[\alpha/\text{Fe}]$ – $[\text{Fe}/\text{H}]$  distribution can reveal about the formation of the galaxy, both in terms of the  $\alpha$ -abundance ratios of individual GCs and where in  $[\alpha/\text{Fe}]$ – $[\text{Fe}/\text{H}]$  space we should look for remnants of disrupted GCs.

Many works present the hypothesis that GCs should follow the  $[\alpha/\text{Fe}]$ – $[\text{Fe}/\text{H}]$  distribution of field stars and those GCs that have been accreted should show relatively low  $[\alpha/\text{Fe}]$  for their  $[\text{Fe}/\text{H}]$ . We show in Fig. 2 that the GCs do follow the general trend of the field stars and if we were to observe a GC with a low  $[\alpha/\text{Fe}]$  abundance, then it is likely that this GC has been recently accreted alongside a dwarf galaxy. However, it is impossible to distinguish between *in situ* GCs and GCs that were accreted early in the formation history of the galaxy based on  $\alpha$ -enhancement alone.

When focusing on the field star  $[\alpha/\text{Fe}]$ – $[\text{Fe}/\text{H}]$  distribution, there is a wide range of shapes, from a smooth decline to clearly bimodal (Fig. 1). The high- $\alpha$  field star sequence present in some of our galaxies is made up of a large fraction of disrupted GCs (Fig. 3). This is due to the high pressure environment that is necessary to create a high  $[\alpha/\text{Fe}]$  sequence. This environment creates very short gas consumption times ( $T_g$ ), making it ideal for GC formation and, due to the ‘cruel cradle effect’, subsequent destruction. This area of high  $[\alpha/\text{Fe}]$  is located close to the centre of the galaxy and we therefore calculate the fraction of disrupted GCs contributing to the bulge of each of the 25 galaxies ( $f_{\text{bulge}}$ ).

Fig. 4 shows that the galaxies which show the strongest bimodality also show rapid early growth of their progenitors. It is also the most bimodal galaxies that have the highest contribution from disrupted clusters,  $f_{\text{bulge}}$ . Mackereth et al. (2018) showed that a high- $\alpha$  sequence in MW-like galaxies is formed via a phase of rapid early formation, a conclusion that is corroborated by our comparison of the  $f_{\text{bulge}}$ – $z_{\text{formation}}$  relation with the high  $f_{\text{bulge}}$  fraction inferred by Schiavon et al. (2017). We also add that galaxies that formed, on average, earlier than typical galaxies of that mass, are likely to have a relatively high fraction of stars in the bulge that originated in GCs. It is the high- $\alpha$  sequence in these galaxies are likely to contain a high fraction of stars that were born in GCs.

We compare the  $f_{\text{bulge}}$  of the E-MOSAICS galaxies to that of the MW and find that the MW has an unusually high  $f_{\text{bulge}}$ , comparable to only 2 out of the 25 E-MOSAICS galaxies. This is consistent with the conclusions of previous works that the MW underwent a period of rapid growth early in its formation, suggesting that its mass assembly history is atypical of  $L_*$  galaxies (e.g. Mackereth et al. 2018; Kruijssen et al. 2019b).

## ACKNOWLEDGEMENTS

We thank the anonymous reviewer for a positive report that improved the clarity of this paper. JP and NB gratefully acknowledge funding from a European Research Council consolidator grant (ERC-CoG-646928-Multi-Pop). JMDK gratefully acknowledges funding from the German Research Foundation (DFG) in the form

of an Emmy Noether Research Group (grant number KR4801/1-1). JMDK and MRC gratefully acknowledge funding from the European Research Council (ERC) under the European Unions Horizon 2020 research and innovation programme via the ERC Starting Grant MUSTANG (grant number 714907). MRC is supported by a Fellowship from the International Max Planck Research School for Astronomy and Cosmic Physics at the University of Heidelberg (IMPRS-HD). NB and RAC are Royal Society University Research Fellows. This work used the DiRAC Data Centric system at Durham University, operated by the Institute for Computational Cosmology on behalf of the STFC DiRAC HPC Facility ([www.dirac.ac.uk](http://www.dirac.ac.uk)). This equipment was funded by BIS National E-infrastructure capital grant ST/K00042X/1, STFC capital grants ST/H008519/1 and ST/K00087X/1, STFC DiRAC Operations grant ST/K003267/1, and Durham University. DiRAC is part of the National E-Infrastructure. The study also made use of high performance computing facilities at Liverpool John Moores University, partly funded by the Royal Society and LJMU’s Faculty of Engineering and Technology.

## REFERENCES

- Abadi M. G., Navarro J. F., Steinmetz M., Eke V. R., 2003, *ApJ*, 597, 21  
 Adamo A., Bastian N., 2018, in *Stahler S., ed., Astrophysics and Space Science Library*, Vol. 424, *The Birth of Star Clusters*. Springer International Publishing, p. 91  
 Adamo A., Kruijssen J. M. D., Bastian N., Silva-Villa E., Ryon J., 2015, *MNRAS*, 452, 246  
 Adibekyan V. Z., Sousa S. G., Santos N. C., Delgado Mena E., González Hernández J. I., Israelian G., Mayor M., Khachatryan G., 2012, *A&A*, 545, A32  
 Antonini F., 2013, *ApJ*, 763, 62  
 Bastian N., 2008, *MNRAS*, 390, 759  
 Bastian N., 2016, in *Morax E., Lebreton Y., Charbonnel C., eds, EAS Publ. Ser. Vol. 80*. p. 5  
 Bastian N., Lardo C., 2018, *ARA&A*, 56, 83  
 Bellazzini M., Ferraro F. R., Ibata R., 2003, *AJ*, 125, 188  
 Buder S. et al., 2018, *MNRAS*, 478, 4513  
 Carollo D., Martell S. L., Beers T. C., Freeman K. C., 2013, *ApJ*, 769, 87  
 Carretta E. et al., 2009, *A&A*, 505, 117  
 Cleveland W. S., 1979, *J. Am. Stat. Assoc.*, 74, 829  
 Cohen J. G., 2004, *AJ*, 127, 1545  
 Crain R. A. et al., 2015, *MNRAS*, 450, 1937  
 D’Ercole A., Vesperini E., D’Antona F., McMillan S. L. W., Recchi S., 2008, *MNRAS*, 391, 825  
 Da Costa G. S., Armandroff T. E., 1995, *AJ*, 109, 2533  
 Davies J. J., Crain R. A., McCarthy I. G., Oppenheimer B. D., Schaye J., Schaller M., McAlpine S., 2019, *MNRAS*, 485, 3783  
 De Lucia G., Springel V., White S. D. M., Croton D., Kauffmann G., 2006, *MNRAS*, 366, 499  
 De Silva G. M. et al., 2015, *MNRAS*, 449, 2604  
 Dinescu D. I., Majewski S. R., Girard T. M., Cudworth K. M., 2000, *AJ*, 120, 1892  
 Dolag K., Borgani S., Murante G., Springel V., 2009, *MNRAS*, 399, 497  
 Fernández-Trincado J. G. et al., 2019, preprint ([arXiv:1904.05884](https://arxiv.org/abs/1904.05884))  
 Forbes D. A., Bridges T., 2010, *MNRAS*, 404, 1203  
 Freeman K., Bland-Hawthorn J., 2002, *ARA&A*, 40, 487  
 Fuhrmann K., 1998, *A&A*, 338, 161  
 Gieles M. et al., 2018, *MNRAS*, 478, 2461  
 Gilmore G. et al., 2012, *Messenger*, 147, 25  
 Grand R. J. J. et al., 2018, *MNRAS*, 474, 3629  
 Gratton R., Sneden C., Carretta E., 2004, *ARA&A*, 42, 385  
 Hayden M. R. et al., 2015, *ApJ*, 808, 132

- Hughes M. E., Pfeffer J., Martig M., Bastian N., Crain R. A., Kruijssen J. M. D., Reina-Campos M., 2019, *MNRAS*, 482, 2795
- Kruijssen J. M. D., 2012, *MNRAS*, 426, 3008
- Kruijssen J. M. D., 2014, *Class. Quantum Gravity*, 31, 244006
- Kruijssen J. M. D., Pelupessy F. I., Lamers H. J. G. L. M., Portegies Zwart S. F., Icke V., 2011, *MNRAS*, 414, 1339
- Kruijssen J. M. D., Maschberger T., Moeckel N., Clarke C. J., Bastian N., Bonnell I. A., 2012, *MNRAS*, 419, 841
- Kruijssen J. M. D., Pfeffer J. L., Crain R. A., Bastian N., 2019a, *MNRAS*, 486, 3134
- Kruijssen J. M. D., Pfeffer J. L., Reina-Campos M., Crain R. A., Bastian N., 2019b, *MNRAS*, 486, 3180
- Larsen S. S., Brodie J. P., Strader J., 2012, *A&A*, 546, A53
- Law D. R., Majewski S. R., 2010, *ApJ*, 714, 229
- Lee J.-W., López-Morales M., Carney B. W., 2006, *ApJ*, 646, L119
- Lin D. N. C., Richer H. B., 1992, *ApJ*, 388, L57
- Longmore S. N., et al., 2014, *Protostars and Planets VI*, University of Arizona Press, p. 291
- Mackereth J. T., Crain R. A., Schiavon R. P., Schaye J., Theuns T., Schaller M., 2018, *MNRAS*, 477, 5072
- Madau P., Dickinson M., 2014, *ARA&A*, 52, 415
- Majewski S. R. et al., 2017, *AJ*, 154, 94
- Marino A. F. et al., 2012, *ApJ*, 746, 14
- Martell S. L., Smolinski J. P., Beers T. C., Grebel E. K., 2011, *A&A*, 534, A136
- Martell S. L. et al., 2016, *ApJ*, 825, 146
- Martocchia S. et al., 2018a, *MNRAS*, 473, 2688
- Martocchia S., et al., 2018b, *MNRAS*, 477, 4696
- Massari D., Koppelman H. H., Helmi A., 2019, *A&A*, 630, L4
- Matteucci F., Brocato E., 1990, *ApJ*, 365, 539
- McWilliam A., 1997, *ARA&A*, 35, 503
- Mistani P. A. et al., 2016, *MNRAS*, 455, 2323
- Monaco L., Saviane I., Correnti M., Bonifacio P., Geisler D., 2011, *A&A*, 525, A124
- Mucciarelli A., Bellazzini M., Catelan M., Dalessandro E., Amigo P., Correnti M., Cortés C., D’Orazi V., 2013, *MNRAS*, 435, 3667
- Pfeffer J., Kruijssen J. M. D., Crain R. A., Bastian N., 2018, *MNRAS*, 475, 4309
- Price-Jones N., Bovy J., 2019, *MNRAS*, 487, 871
- Pritzl B. J., Venn K. A., Irwin M., 2005, *AJ*, 130, 2140
- Qu Y. et al., 2017, *MNRAS*, 464, 1659
- Reina-Campos M., Kruijssen J. M. D., 2017, *MNRAS*, 469, 1282
- Reina-Campos M., Hughes M. E., Kruijssen J. M. D., Pfeffer J., Bastian N., Crain R. A., Koch A., Grebel E. K., 2019a, preprint ([arXiv:1910.06973](https://arxiv.org/abs/1910.06973))
- Reina-Campos M., Kruijssen J. M. D., Pfeffer J. L., Bastian N., Crain R. A., 2019b, *MNRAS*, 486, 5838
- Sakari C., Venn K., Arimoto N., Aoki W., Irwin M., 2011, *American Astronomical Society Meeting Abstracts #217.000*, p. 434.48
- Sales L. V. et al., 2015, *MNRAS*, 447, L6
- Schaye J., Dalla Vecchia C., 2008, *MNRAS*, 383, 1210
- Schaye J. et al., 2015, *MNRAS*, 446, 521
- Schechter P., 1976, *ApJ*, 203, 297
- Schiavon R. P. et al., 2017, *MNRAS*, 465, 501
- Segers M. C., Schaye J., Bower R. G., Crain R. A., Schaller M., Theuns T., 2016, *MNRAS*, 461, L102
- Siebert A. et al., 2011, *AJ*, 141, 187
- Snedden C., 2004, *Mem. Soc. Astron. Italiana*, 75, 267
- Springel V., White S. D. M., Tormen G., Kauffmann G., 2001, *MNRAS*, 328, 726
- Steinmetz M. et al., 2006, *AJ*, 132, 1645
- Tacconi L. J. et al., 2018, *ApJ*, 853, 179
- Tautvaišienė G., Wallerstein G., Geisler D., Gonzalez G., Charbonnel C., 2004, *AJ*, 127, 373
- Ting Y.-S., Conroy C., Goodman A., 2015, *ApJ*, 807, 104
- Tolstoy E., Hill V., Tosi M., 2009, *ARA&A*, 47, 371
- Usher C., Pfeffer J., Bastian N., Kruijssen J. M. D., Crain R. A., Reina-Campos M., 2018, *MNRAS*, 480, 3279
- Wheeler J. C., Sneden C., Truran J. W., Jr, 1989, *ARA&A*, 27, 279
- Wiersma R. P. C., Schaye J., Smith B. D., 2009, *MNRAS*, 393, 99
- Zwitter T. et al., 2008, *AJ*, 136, 421

## APPENDIX: LINK BETWEEN BIMODALITY AND GAS CONSUMPTION TIME

The high [O/Fe] sequence observed in some of the E-MOSAICS galaxies can be explained via a high pressure natal environment. In a high-density (pressure) environment, the gas consumption time-scale of the natal gas is short, and therefore the natal gas is consumed before it can be enriched with the Fe nucleosynthesized by Type-Ia SNe. Mackereth et al. (2018) shows that the amount of  $\alpha$ -enhancement correlates with the gas consumption time-scale ( $t_g$ ) of field stars. We now test this for the GCs and field stars in the 25 E-MOSAICS galaxies. The consumption time of the natal gas from which the GC formed is calculated, following the description in Schaye & Dalla Vecchia (2008, equation 11) as

$$t_g = A^{-1} (1 M_{\odot} \text{pc}^{-2})^n \left( \frac{\gamma}{G} f_g P_{\star} \right)^{(1-n)/2}. \quad (\text{A1})$$

Here, the parameters  $A = 1.515 \times 10^{-4} M_{\odot} \text{yr}^{-1} \text{kpc}^{-2}$  and  $n = 1.4$  are specified by observations (see Schaye et al. 2015 for details).  $\gamma = 5/3$  is the ratio of specific heats for an ideal gas,  $f_g$  is the local gas fraction (assumed to be unity), and  $P_{\star}$  is the pressure of the natal gas.  $t_g$  provides an estimate of the amount of time a star-forming gas particle resides in the ISM before becoming a star particle (though we note this is an over-estimate since it neglects ejection of the ISM in winds), a low  $t_g$  therefore indicates vigorous star formation.

Following the methodology used by Davies et al. (2019), for each of the galaxies we compute the running median of the [O/Fe]–[Fe/H] relation and the  $t_g$ –[Fe/H] relation using the locally weighted scatter plot smoothing method (LOWESS; Cleveland 1979). The running medians are calculated separately for the stars, GCs, and initial GCs. We then compute the difference from these running medians for each GC and star, i.e.  $\Delta t_{g,\text{GC}} = t_{g,\text{GC}} - t_{g,\text{GC,median}}$ . The correlation between  $\Delta[\text{O/Fe}]$  and  $\Delta t_g$  is computed as a Spearman rank correlation coefficient ( $\rho$ ).

The top row of Fig. A1 shows the  $z = 0$  GCs along with the running medians (black lines) for each of the galaxies. Each GC is coloured by the consumption time of its natal gas ( $t_g$ ). The bottom panels of Fig. A1 show the Spearman- $\rho$  values for the  $z = 0$  GCs shown in the top panels and also the initial GCs and the field stars. Here, the  $z = 0$  GCs are those that survive until present day with a mass  $> 10^5 M_{\odot}$ , the initial GCs are those that were formed with a mass  $> 10^5 M_{\odot}$  but do not necessarily survive until  $z = 0$ .

In the left and the middle panels of Fig. A1, the  $\rho$ -values are calculated in 15 equally sized bins from  $-2.5 < [\text{Fe/H}] < 0.5$ . In the right-hand panel, the  $\rho$ -values are calculated in 10 equally sized bins across the same metallicity range, to account for lower number statistics. The Spearman  $p$ -value is indicative as to whether a correlation is significant as it depends on the strength of the correlation and the sample size. We calculate the  $p$ -value for each of the bins and shade the bins to highlight, where the  $\Delta[\text{O/Fe}]$ – $\Delta t_g$  correlation is not significant (the Spearman  $p$ -value exceeds 0.01). For the  $z = 0$  GCs, the correlation for the initial GCs and the stars is significant everywhere. The galaxies are grouped by the shape of their field star contours in [O/Fe]–[Fe/H] space (as discussed in Section 5) and from left to right show: no bimodality, intermediate bimodality, and clear bimodality.

Inspection by eye shows that, in the top panels, the GCs that have a higher than average [O/Fe] have a lower than average  $t_g$ . Hence,

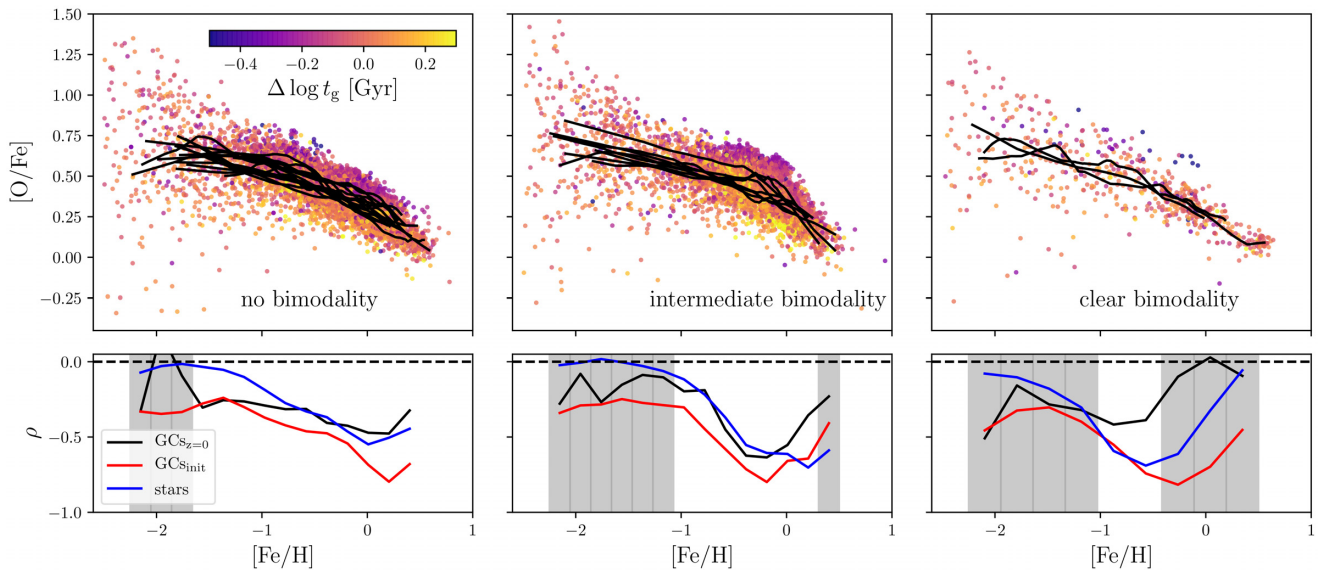


**Figure A1.** Top row: The  $[O/Fe]$ – $[Fe/H]$  relation for GCs grouped by their galaxy’s degree of bimodality. The solid black lines represent the running medians of the individual galaxies, computed using the LOWESS method. Each point represents one  $z = 0$  GC coloured by its difference from the running median of the  $t_g$ – $[Fe/H]$  relation of its host galaxy. Bottom row: The Spearman rank correlation coefficient of the  $\Delta t_g$ – $\Delta[O/Fe]$  relation. Each line represents present-day GCs ( $GC_{S_{z=0}}$ , black), any GC that formed ( $GC_{S_{init}}$ , red) and the field stars (blue). The shaded regions highlight the metallicity bins in which the Spearman correlation coefficient for  $GC_{S_{z=0}}$  is not significant (Spearman  $p$ -value  $> 0.01$ ). The other populations have significant correlations in all  $[Fe/H]$  bins. The  $[Fe/H]$  bins are wider in the clearly bimodal case to account for lower number statistics.

the recovered relation is negatively correlated ( $\rho < 0$ ) for much of the range in  $[Fe/H]$ . Section 4 discusses how the high  $[O/Fe]$  field star sequence in the bimodal galaxies is formed in high pressure environments that induce a short gas consumption time. This is seen directly in Fig. A1, the field stars show a negative correlation everywhere above an  $[Fe/H] > -1$ . However, the correlation is stronger in the intermediate and clearly bimodal galaxies. The initial GCs show the strongest correlation. They show a stronger correlation than the field stars because some stars that form with fast consumption times are  $\alpha$ -poor, this therefore weakens the field star correlation.

As discussed in Section 4, the high pressures that create the most  $\alpha$ -rich stars in the clearly bimodal galaxies creates the perfect environment to form and then subsequently destroy high- $\alpha$  GCs. Again this can be seen directly in Fig. A1. In the lower right-hand

panel, the initial GCs show a strong negative correlation between their  $\alpha$ -enhancement and relative  $t_g$ . However, the GCs that survive until the present day do not show such a relation, because many of the GCs with the shortest  $t_g$  have been destroyed. All galaxies show a weaker correlation between  $\Delta[O/Fe]$  and  $\Delta t_g$  in their  $z = 0$  GCs when compared to their initial GCs, but the difference is most pronounced in the most bimodal galaxies. At  $[Fe/H] = -0.5$  (where the correlation is significant in all galaxies), we calculate the difference in the Spearman  $\rho$ -value between the initial GCs and final GCs for the ‘clearly bimodal’ and ‘no bimodality’ galaxies. The clearly bimodal galaxies have a  $\rho$ -value difference of 0.44, whereas the galaxies with no bimodality have a difference of 0.11.

This paper has been typeset from a  $\text{\TeX}/\text{\LaTeX}$  file prepared by the author.